Non-Linear Compton Scattering of Ultrashort and Ultraintense Laser Pulses

D. Seipt* and B. Kämpfer†

Forschungszentrum Dresden-Rossendorf,

POB 51 01 19, 01314 Dresden, Germany

Abstract

The scattering of temporally shaped intense laser pulses off electrons is discussed by means of manifestly covariant quantum electrodynamics. We employ a framework based on Volkov states with a time dependent laser envelope in light-cone coordinates within the Furry picture. An expression for the cross section is constructed, which is independent of the considered pulse shape and pulse length. A broad distribution of scatted photons with a rich pattern of subpeaks like that obtained in Thomson scattering is found. These broad peaks may overlap at sufficiently high laser intensity, rendering inappropriate the notion of individual harmonics. The limit of monochromatic plane waves as well as the classical limit of Thomson scattering are discussed. As a main result, a scaling law is presented connecting the Thomson limit with the general result for arbitrary kinematics. In the overlapping regions of the spectral density, the classical and quantum calculations give different results, even in the Thomson limit. Thus, a phase space region is identified where the differential photon distribution is strongly modified by quantum effects.

PACS numbers: 12.20.Ds, 41.60.-m

Keywords: high-intensity laser pulses, Compton scattering, Volkov states

* d.seipt@fzd.de

† b.kaempfer@fzd.de

I. INTRODUCTION

The use of chirped-pulse amplification [1] has led to a prodigious advance in available laser power. The current records reach several petawatts, and accompanying interest in strong-field physics culminates in planned large-scale laser facilities such as the anticipated "Extreme Light Infrastructure" (ELI) [2]. The pioneering theoretical studies in strong-field physics considered both pair creation in a strong field [3] and the cross channel process, electron photon scattering [4–10], dubbed non-linear Compton scattering, where the use of laser beams has already been suggested. Since then there has been a wealth of theoretical papers and we refer the reader to the reviews [11–16]. In non-linear Compton scattering

$$e(p) + \ell\gamma_L(k) \to e'(p') + \gamma(k') \tag{1}$$

a number of ℓ photons with momentum k from a high intensity laser, scatter off an electron with momentum p. A convenient measure of laser intensity is the dimensionless laser amplitude $a \equiv eE/m\omega$, with E being the root-mean-square electric field and ω the laser frequency. The parameter a is a purely classical quantity, representing the work performed by the field on the electron in one wavelength. Thus, a is the classical nonlinearity parameter [17] and it is related to the ponderomotive potential $U_p = ma^2/2$. The definition of a can be made explicitly Lorentz and gauge invariant [18]. When a becomes of order unity the quiver motion of the electron in the laser beam becomes relativistic in a classical picture.

The spectrum of non-linear Compton scattering has been observed in several experiments colliding laser and electron beams, such as low-intensity laser photons ($a = 0.01$) with low-energy (~ 1 keV) electrons from an electron gun [19], $a = 2$ photons with plasma electrons from a gas jet [20] and, more recently, sub-terawatt photons ($a = 0.35$) from a CO_2 laser with 60 MeV electrons from a linac at the BNL-ATF [21]. Using linearly polarized photons the latter two experiments [20, 21] have analyzed the characteristic azimuthal intensity distributions confirming quadrupole and sextupole patterns for the second and third harmonics, respectively. Recently, the energy spectrum of the scattered radiation has been measured in an all-optical setup using laser accelerated electrons [22].

Probably the best known experiment is SLAC E-144 probing strong-field QED using a terawatt Nd:glass laser ($a \simeq 0.6$) in conjunction with high-energy (46.6 GeV) electrons [23]. The observation of non-linear Compton scattering has been reported [24] as well as the observation of the crossed process of non-linear pair creation, due to the interaction of a

Compton scattered high-energy photon with a second laser beam [25].

The low-energy limit (in terms of laser frequency) of Compton scattering is Thomson scattering which is described completely classically [26, 27]. This classical picture is used as theoretical framework for many applications of laser Compton scattering such as X-ray sources [28–30] or diagnostic tools [31]. A convenient parameter to distinguish the two regimes is the quantity

$$y_\ell = \frac{s_\ell - m^2}{m^2} = \frac{2\ell k \cdot p}{m^2}, \tag{2}$$

where $s_\ell = (p+\ell k)^2$ expresses the center of mass energy squared for the generation of the ℓth harmonic in a Lorentz invariant manner[1]. The $\ell + 1 \to 2$ process is kinematically equivalent to the scattering of one photon with momentum ℓk off an electron with momentum p, thus it appears as a (pseudo) $2 \to 2$ process. The Thomson regime is recovered for $y_\ell \ll 1$, while for $y_\ell > 1$ one finds striking differences to the Thomson scattering. The electron recoil during the scattering may be quantified by the Lorentz-invariant quantity $t = (p - p')^2$ which is in the range $0 \leq -t \leq m^2 \frac{y_\ell^2}{1+y_\ell}$, i.e. in the Thomson regime $-t/m^2 \ll 1$ holds.

A quantity measuring non-linear quantum effects,

$$\chi_R = \frac{e\sqrt{(F^{\mu\nu}p_\nu)^2}}{m^3} = \frac{1}{2} a y_1, \tag{3}$$

has been introduced in [4, 8]. It measures the work done by the field over the Compton wavelength m^{-1} in the rest frame of the initial electron where the four-vector $p^\mu = (m, 0, 0, 0)$. Introducing the critical field strength [32] $E_S = m^2/e = 1.3 \times 10^{18}$ V/m, this may also be written as $\chi_R = E_\star/E_S$, where $E_\star$ is the rms electric field strength in the electron's rest frame. The parameter χ_R combines nonlinearity and quantum effects. χ_R is of the order of unity if both a and y_1 are of the order of unity. Thus, the corrections to the classical description (Thomson scattering) are important if either (i) an ultraintense high-energy photon pulse, e.g. produced by an X-ray free electron laser, interacts with low-energy electrons, or (ii) a multi-GeV electron beam is brought to collision with an optical high-intensity laser. The latter scenario is similar to the SLAC E-144 experiment but with a higher value of a. For the 50 GeV SLAC beam in conjunction with a counterpropagating optical laser ($\omega \sim 1$ eV) one has $y_\ell \sim 1$. These parameters will be used mainly below for numerical calculations. The

[1] p an k are four-vectors, thus $k \cdot p$ denotes a scalar product; we employ units with $\hbar = c = 1$.

FACET project [33] at SLAC envisages investigations within such kinematics in line with (ii).

Ultraintense lasers use short pulses (few fs, few laser cycles) requiring a proper treatment of the laser pulse structure. Rich substructures of the scattered photon spectra were predicted within the classical picture [34–37] of Thomson scattering. These substructures have not yet been confirmed experimentally. The effect of radiation back reaction on the spectra was studied in [38] and found to be important. Only a few publications address quantum calculations in pulsed fields for scalar particles [39] and for spinor particles [40, 41]. In [42], a connection between the emitted angular spectrum in non-linear Compton scattering and the carrier envelope phase in few-cycle laser pulses was established. In a related field, electron wave-packet dynamics in strong laser fields has been studied in e.g. [43, 44].

In our paper we calculate the emitted photon spectrum in non-linear Compton scattering using a generalized Volkov solution with temporal shape in light-cone coordinates. For this purpose we first focus on the structure of the Volkov wavefunction in a pulsed laser field. The aim of our study is to compare the QED calculations for non-linear Compton scattering with results from a classical calculation, i.e. Thomson scattering.

Our paper is organized as follows. In section II we present Volkov states in pulsed laser fields. Section III continues with the calculation of the matrix element and the transition probability. A slowly varying envelope approximation is discussed. Numerical results are presented in section IV. We discuss various limiting cases of our general results, including monochromatic plane waves and the Thomson limit. As a main result, a scaling law is presented, connecting the Thomson spectrum with the Compton spectrum. In the Appendix we summarize the kinematics in light cone coordinates and present the Fourier transformation of the Volkov state.

II. TEMPORALLY SHAPED VOLKOV STATES

A strong laser field may be considered as a coherent state of photons $|\mathcal{C}\rangle$, characterized by the polarization and momentum distribution $\mathcal{C}^\mu(k)$, if the depletion of the laser photons from $|\mathcal{C}\rangle$ by an interaction process with electrons is negligible, i.e. for any relevant scattering process $S = \langle out; \mathcal{C}'|S|in; \mathcal{C}\rangle$ with $\mathcal{C}' = \mathcal{C}$ is valid, where in and out are particle number states without coherent parts [45]. Then, it is possible to work within the Furry picture [46],

where the interaction of an electron with the classical background field $A^\mu(x)$, which is the Fourier transform of $\mathcal{C}^\mu(k)$, is treated nonperturbatively and solutions of the Dirac equation

$$(i\partial\!\!\!/ - eA\!\!\!/ - m)\psi(x) = 0 \tag{4}$$

are utilized as basic *in* and *out* states for the perturbative expansion of the S matrix. For background fields in the form of plane waves, closed solutions of (4) can be found,

$$\psi_{p,s}(x) = \left(1 + \frac{e}{2k\cdot p} k\!\!\!/ A\!\!\!/\right) \exp\{iS_p(x)\} \frac{u_{p,s}}{\sqrt{2E_p}}, \tag{5}$$

where the free Dirac spinor for momentum p and spin s fulfills $(p\!\!\!/ - m)u_{p,s} = 0$ and is normalized to $\bar{u}_{p,s'}u_{p,s} = 2m\delta_{ss'}$. The phase is the classical Hamilton Jacobi action

$$S_p(x) = -p\cdot x + f(k\cdot x), \tag{6}$$

with $f = f_1 + f_2$, $f_1 = -\int\limits_{\phi_0}^{k\cdot x} \mathrm{d}\phi \frac{eA\cdot p}{k\cdot p}$ and $f_2 = \int\limits_{\phi_0}^{k\cdot x} \mathrm{d}\phi \frac{e^2A^2}{2k\cdot p}$. Equation (5) represents the famous Volkov states, whose perturbative expansion in terms of interactions with the laser field is depicted in figure 1 of [45] (The expansion parameter, i.e. the coupling strength at the vertices, is a_0 defined below).

For the vector potential we use a real transverse plane wave

$$A^\mu = A_0\, g(k\cdot x)\, (\epsilon_1^\mu \cos\xi \cos k\cdot x + \epsilon_2^\mu \sin\xi \sin k\cdot x), \tag{7}$$

modified by an envelope function g and fulfilling $A\cdot k = 0$ and $k\cdot k = 0$. The parameter ξ determines the polarization of the laser: It is linearly $x\,(y)$ polarized for $\xi = 0\,(\xi = \pi/2)$ and circularly polarized for $\xi = \pm\pi/4$. For other values of ξ, the laser is elliptically polarized [47]. The vector potential is normalized such that the mean energy density or the energy flux $\langle \mathbf{E}^2\rangle \propto -A_\mu A^\mu = g^2A_0^2/2$, where $\langle\ldots\rangle$ means averaging over the fast oscillations of the carrier wave, is independent of ξ, but the dimensionless laser amplitude a, as defined in the introduction, is time dependent. A time independent laser strength parameter may be defined by the normalized peak value of the vector potential $a_0 = eA_0/m$ (with this definition, $a^2 = a_0^2/2$ for $g \equiv 1$). The vector potential (7) can also be cast into a complex form

$$A^\mu = \frac{A_0 g(k\cdot x)}{2}(\epsilon_+^\mu e^{-ik\cdot x} + \epsilon_-^\mu e^{+ik\cdot x}) = \frac{A_0 g}{2} B^\mu, \tag{7'}$$

with the complex polarization vectors $\epsilon_\pm^\mu = \cos\xi\epsilon_1^\mu \pm i\sin\xi\epsilon_2^\mu$ with $\epsilon_+\cdot\epsilon_- = -1$, $\epsilon_\pm\cdot\epsilon_\pm = \sin^2\xi - \cos^2\xi$ and the definition $B^\mu = \epsilon_+^\mu e^{-ik\cdot x} + \epsilon_-^\mu e^{+ik\cdot x}$.

In what follows, the temporal pulse shape will often be chosen as a *cosh* pulse

$$g(k\cdot x) = \frac{1}{\cosh\left(\dfrac{k\cdot x}{\sigma}\right)}, \tag{8}$$

with width σ, or a Gaussian

$$g(k\cdot x) = \exp\left\{-\frac{(k\cdot x)^2}{2\sigma^2}\right\}. \tag{9}$$

Besides these special cases, any other smooth function g which depends solely on $k\cdot x$ is possible.

Since the vector potential A^μ depends only on $k\cdot x$, it is convenient to work in light-cone coordinates with $k\cdot x = \omega x_+$ (see Appendix A). In these coordinates, the Volkov wavefunction (5) reads

$$\psi_{p,s}(x) = C_p(\mathbf{x}_\perp, x_-, x_+)\frac{u_{p,s}}{\sqrt{2E_p}}, \tag{10}$$

$$C_p(\mathbf{x}_\perp, x_-, x_+) = \left[1 + d_p g(x_+)\left(\not{k}\not{\epsilon}_- e^{i\omega x_+} + \not{k}\not{\epsilon}_+ e^{-i\omega x_+}\right)\right] e^{-\frac{i}{2}(p_+x_- + p_-x_+) + i\mathbf{p}_\perp\cdot\mathbf{x}_\perp + if(x_+)} \tag{11}$$

with $d_p = a_0 m/(4k\cdot p)$. For many purposes it is sufficient to consider only the function C_p since it contains the relevant information on the interaction of the electron with the laser pulse. The real part[2] of the scalar projection $\mathcal{S} = \frac{1}{4}\mathrm{tr}\, C_p(x) = \exp\{iS_p(x)\}$ is visualized in Fig. 1 in the frame where the electron is initially at rest. The scalar projection is essentially equivalent to probing the state $\psi_{p,s}$ with $\bar{u}_{p,s}$ and an average over the spins s

$$\frac{1}{2}\sum_s \frac{\bar{u}_{p,s}}{\sqrt{2E_p}}\psi_{p,s}(x) = \frac{m}{E_p}\mathcal{S}. \tag{12}$$

In that frame the (free) electron wavefunction outside the laser pulse behaves as $\propto e^{-ip\cdot x} = e^{-imt}$. The effect of the laser pulse is a local deformation of the electron wavefronts due to the build-up of an effective, time dependent momentum $q^\mu(x_+) = p^\mu + g^2(x_+)b_p k^\mu$ with $b_p = m^2 a_0^2/4k\cdot p$. The momentum $q^\mu(x_+)$ achieves its maximum at the center of the laser pulse $x_+ = 0$, depicted as diagonal straight line in Fig. 1, where it coincides with the usual quasi momentum in monochromatic plane waves. Thus, inside the laser pulse, especially

[2] The imaginary part gives no further information; it has a shifted phase as compared to the real part.

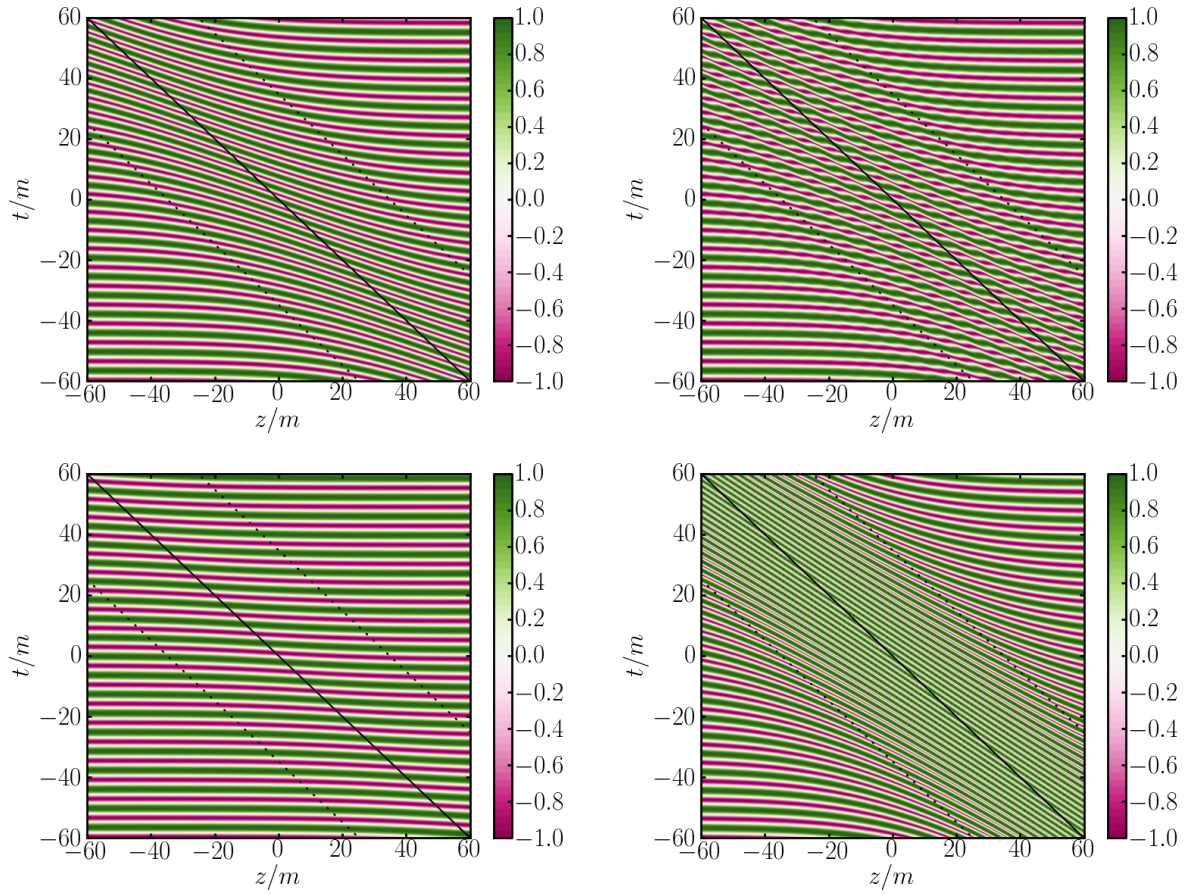

Figure 1. Contour plot of $\frac{1}{4}\mathrm{tr}\, C_p(x)$ in position space in the $z-t$ plane. The laser pulse with *cosh* profile is located between the two dotted lines. Left (right) top panel: Circularly (linearly) polarized laser pulse with $a_0 = 1.5$ and $\sigma = 20$, Bottom panels: circular polarization for $a_0 = 0.5$ (left) and $a_0 = 3.0$ (right).

for $x_+ = 0$, the fully dressed electron wavefunction behaves as $\propto e^{-iq\cdot x} = e^{-i(m+b_p\omega_\star)t+ib_p\omega_\star z}$, i.e. the electron wavelength changes and the wavefronts become tilted. Both effects are proportional to the ponderomotive potential, i.e. $\propto b_p\omega_\star = ma_0^2/4 = U_p/2$, where $\omega_\star = u\cdot k$ is the laser frequency in the initial electron rest frame and $u = p/m$. In Fig. 1, $\omega_\star = 300$ keV is chosen which can be achieved, for instance, with laser photons of 1.5 eV energy colliding head-on with 50 GeV electrons, or a 15 keV X-ray laser beam with 5 MeV electrons. The electron wavefunction changes its behavior from the free case to the fully dressed case over $N = \sigma m/(2\pi\omega_\star)$ oscillations of the free electron wavefunction, i.e. $N = 5.5$ for the parameters employed in Fig. 1. For lower values of $\omega_\star$, the behavior of the electron wavefunction changes slowly over many oscillations, e.g. for $\omega_\star = 200$ eV (35 MeV electrons colliding with 1.5 eV

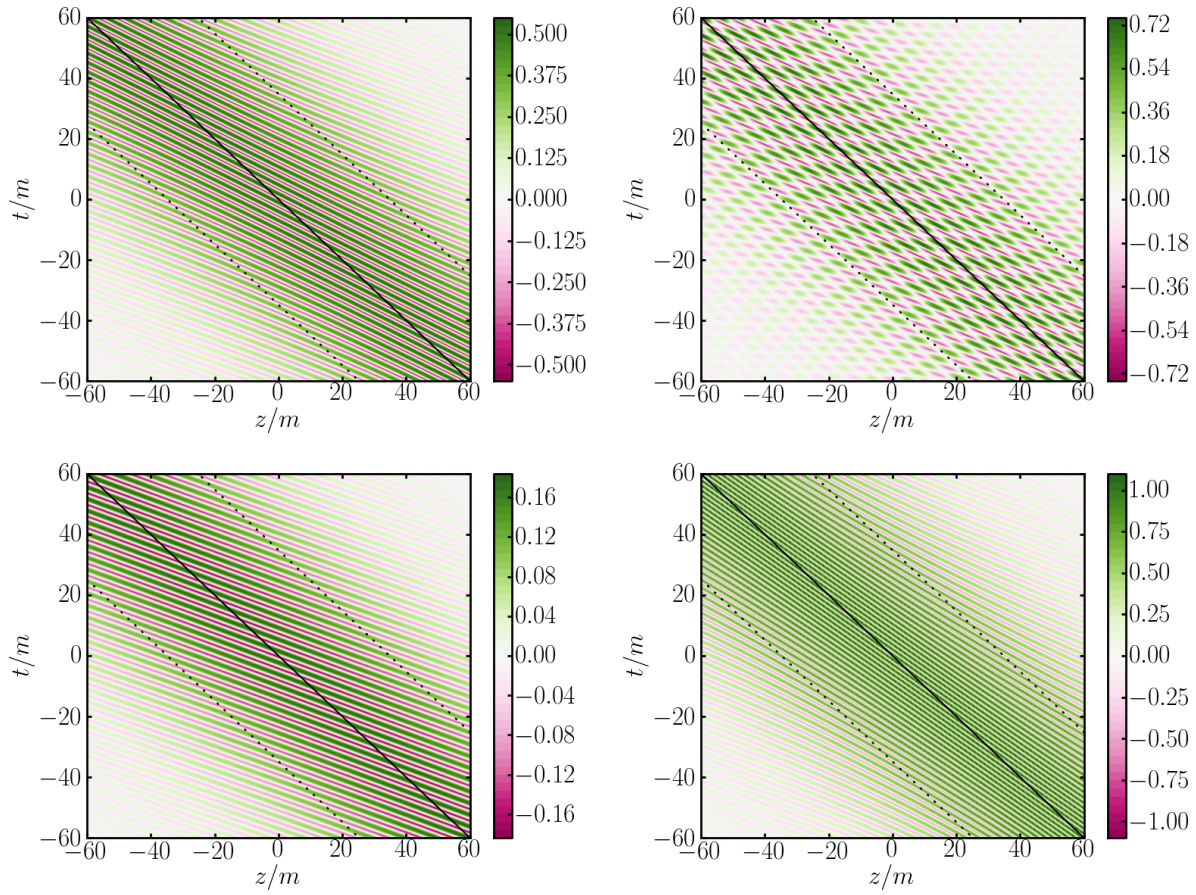

Figure 2. Contour plot of the spin flip contribution to the Volkov wave function by the tensor projection $\mathcal{T}^{13} - i\mathcal{T}^{23}$. Same parameters as in Fig. 1.

photons) and $\sigma = 20$ one finds $N = 8100$. For a linearly polarized laser, additional ripples appear in the interaction region due to the oscillating terms in the phase. For non-head-on geometries, similar ripples are also present for circular polarization. The smoothness of the pulse envelope g ensures the smoothness of the Volkov wavefunction in the transition from the field-free regions to the laser pulse.

Vector projections with an odd number of Dirac matrices, such as $\mathcal{V}^\mu = \frac{1}{4}\mathrm{tr}\,\gamma^\mu C_p(x)$ or $\mathcal{A}^\mu = \frac{1}{4}\mathrm{tr}\,\gamma^5\gamma^\mu C_p(x)$, vanish identically and are, therefore, not useful for characterizing $\psi_{p,s}$. The pseudoscalar $\mathcal{P} = \frac{1}{4}\mathrm{tr}\,\gamma^5 C_p(x)$ also vanishes. The antisymmetric tensor projections $\mathcal{T}^{\mu\nu} = \frac{1}{4}\mathrm{tr}\,\sigma^{\mu\nu} C_p(x) = id_p(k^\nu A^\mu - k^\mu A^\nu)\exp\{iS_p(x)\}$, where $\sigma^{\mu\nu} = \frac{i}{2}[\gamma^\mu, \gamma^\nu]$ is the spin tensor, allow for a further characterization by $\sigma^{01}, \sigma^{02}, \sigma^{13}, \sigma^{23}$ for circular laser polarization and for σ^{01}, σ^{13} for linear polarization. These tensor projections are nonzero but only inside the laser pulse. They mix contributions with different spin orientation and are therefore propor-

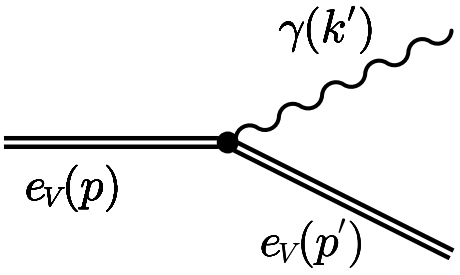

Figure 3. Feynman diagram for non-linear Compton scattering as the decay of a laser dressed Volkov electron state.

tional to a combination of $\bar{u}_{p,1}\psi_{p,2}(x)$ and $\bar{u}_{p,2}\psi_{p,1}(x)$, i.e. the spin-up wavefunction contains contributions with spin-down and vice versa. From the structure of the Pauli interaction term $\sigma^{\mu\nu}F_{\mu\nu}$, where $F_{\mu\nu} = \partial_\mu A_\nu - \partial_\nu A_\mu$ is the electromagnetic field strength tensor, one can infer that σ^{01} (σ^{02}) corresponds to the interaction of the electron with the x (y) component of the electric field, and σ^{13} (σ^{23}) corresponds to the y (x) component of the magnetic field. From this correspondence and by inspecting (7) it is easy to understand why some projections are zero for linear polarization while they are nonzero for circular polarization. As an example, the tensor projection $\mathcal{T}^{13} - i\mathcal{T}^{23}$ is shown in Fig. 2.

III. CALCULATION OF THE MATRIX ELEMENT

A. The S matrix

The interaction of the Volkov electron e_V with photon modes different from the laser field are treated by perturbative S matrix expansion. The Born approximation of the matrix element for the emission of one photon, i.e. non-linear Compton scattering $e_V(p) \to e_V(p') + \gamma(k')$, is depicted in Fig. 3. Using Feynman rules [48], the S matrix element for such a process is given by

$$S_{fi} = \langle p', s'; k', \epsilon'_{\lambda'}|S[A]|p, s\rangle = -ie\int \mathrm{d}^4x\bar{\psi}_{p',s'}(x)\frac{e^{ik'\cdot x}}{\sqrt{2\omega'}}\not{\epsilon}'_{\lambda'}\psi_{p,s}(x), \tag{13}$$

which reads in light-cone coordinates, suppressing spin (s, s') and polarization (λ') indices from now on,

$$S_{fi} = N_0 \int \mathrm{d}^4x \bar{u}_{p'} \big(1 + d_{p'} \not{B} \not{k}\big) \not{\epsilon}' \big(1 + d_p \not{k} \not{B}\big) u_p e^{i(S_p - S_{p'} + ik'\cdot x)} \tag{14}$$

$$= \frac{N_0}{2} \int \mathrm{d}^2\mathbf{x}_\perp \, \mathrm{d}x_+ \, \mathrm{d}x_- \, \Gamma(x_+) e^{iH(x_+, x_-, \mathbf{x}_\perp)} \tag{15}$$

with $N_0 = -ie/\sqrt{2\omega' 2E_p 2E_{p'}}$ and

$$\Gamma(x_+) = \mathscr{T}_0^0 + g\, e^{i\omega x_+} \mathscr{T}_1^1 + g\, e^{-i\omega x_+} \mathscr{T}_{-1}^1 + g^2\, \mathscr{T}_0^2 + g^2\, e^{2i\omega x_+} \mathscr{T}_2^2 + g^2\, e^{-2i\omega x_+} \mathscr{T}_{-2}^2, \tag{16}$$

where

$$\mathscr{T}_0^0 = \bar{u}_{p'} \not{\epsilon}' u_p, \tag{17}$$

$$\mathscr{T}_{\pm 1}^1 = \bar{u}_{p'} \left(d_{p'} \not{\epsilon}_\mp \not{k} \not{\epsilon}' + d_p \not{\epsilon}' \not{k} \not{\epsilon}_\mp \right) u_p, \tag{18}$$

$$\mathscr{T}_0^2 = 4(k\cdot\epsilon') d_p d_{p'} \bar{u}_{p'} \not{k} u_p, \tag{19}$$

$$\mathscr{T}_{\pm 2}^2 = d_p d_{p'} \bar{u}_{p'} \left(\not{\epsilon}_\mp \not{k} \not{\epsilon}' \not{k} \not{\epsilon}_\mp \right) u_p. \tag{20}$$

Due to $\not{\epsilon}_\mp \not{k} \not{\epsilon}' \not{k} \not{\epsilon}_\mp = -2(\epsilon'\cdot k)(\epsilon_\mp \cdot \epsilon_\mp) \not{k}$, one finds $\mathscr{T}_{\pm 2}^2 = 0$ for circular polarization. Furthermore,

$$\begin{aligned} H(x_+, x_-, \mathbf{x}_\perp) &= S_p - S_{p'} + ik'\cdot x \\ &= (p' + k' - p)\cdot x + f(x_+) - f'(x_+) \end{aligned} \tag{21}$$

with $f' = f(p \to p') = f_1(p') + f_2(p')$ and

$$f_1(x_+; p) = \frac{m a_0}{k\cdot p} \int_{\phi_0}^{k\cdot x} \mathrm{d}\phi \, g(\phi) \left[p\cdot\epsilon_1 \cos\xi \cos\phi + p\cdot\epsilon_2 \sin\xi \sin\phi \right], \tag{22}$$

$$f_2(x_+; p) = -\frac{m^2 a_0^2}{2k\cdot p} \int_{\phi_0}^{k\cdot x} \mathrm{d}\phi \, g^2(\phi) \big[\cos^2\xi \cos^2\phi + \sin^2\xi \sin^2\phi \big]. \tag{23}$$

Inspecting Eq. (21), it is obvious that the dependence of H on x_- and $\mathbf{x}_\perp$ is trivial and the integrations over these variables in Eq. (15) can be done analytically. As a result, energy-momentum conservation is imposed on the components P_+ and $\mathbf{P}_\perp$, and the exponent

$$H_+(x_+) = \frac{1}{2}(k'_- + p'_- - p_-)x_+ + f(x_+) - f'(x_+) \tag{24}$$

remains. Due to the non-trivial pulse dependent structure of H_+, the x_+ integration does not yield another conservation law. Thus, the frequency of scattered photons ω' is not fixed

by energy and momentum conservation as a function of scattering angle θ and remains as independent parameter. Including the x_+ dependence of $\Gamma(x_+)$, some rather complicated functions of ω' emerge

$$\mathscr{A}_N^M = \int_{-\infty}^{\infty} \mathrm{d}x_+ g^M(x_+) \exp i\{H_+(x_+) + N\omega x_+\}. \tag{25}$$

With these definitions, the S matrix element can be written as

$$S_{fi} = (2\pi)^3 \delta^2(\mathbf{k}'_\perp + \mathbf{p}'_\perp - \mathbf{p}_\perp)\delta(k'_+ + p'_+ - p_+) N_0 \mathscr{M} \tag{26}$$

with

$$\mathscr{M} = \mathscr{T}_0^0 \mathscr{A}_0^0 + \mathscr{T}_1^1 \mathscr{A}_1^1 + \mathscr{T}_{-1}^1 \mathscr{A}_{-1}^1 + \mathscr{T}_0^2 \mathscr{A}_0^2 + \mathscr{T}_2^2 \mathscr{A}_2^2 + \mathscr{T}_{-2}^2 \mathscr{A}_{-2}^2. \tag{27}$$

The integrals $\mathscr{A}_N^M$ are numerically convergent for $M \geq 1$ due to the presence of the pulse function in the integrand, rendering the range of integration practically finite. The integral $\mathscr{A}_0^0$, however, contains a divergent part and must be regularized. A possible method has been proposed in [41], where one multiplies the integrand with a convergence factor $e^{-\varepsilon|x_+|}$, $\varepsilon > 0$, and performs an integration by parts. The result is

$$\mathscr{A}_0^0 = -\frac{2}{P_-} \int_{-\infty}^{\infty} \mathrm{d}x_+ \frac{\mathrm{d}(f - f')}{\mathrm{d}x_+} \exp\{iH_+(x_+)\} + 4e^{i[f(0)-f'(0)]} \lim_{\varepsilon \to 0^+} \frac{\varepsilon}{P_-^2 + \varepsilon^2}, \tag{28}$$

with $P_- = k'_- + p'_- - p_-$. In (28), the first part is now convergent and the second part is proportional to a δ distribution with support at $\omega' = 0$. The latter contribution can be neglected in our analysis for $\omega' > 0$. This regularized version of $\mathscr{A}_0^0$ will be used in the subsequent numeric calculations.

B. Slowly Varying Envelope Approximation

The calculations are simplified upon utilizing the slowly varying envelope approximation (SVEA) of the phase of the $\mathscr{A}_N^M$ functions. This approximation scheme is suitable for long pulses with $\sigma \gg 1$. Typically σ is proportional to the number of laser oscillations under the envelope. For f_1, which is proportional to g (see Eq. (22)), an integration by parts is performed, yielding

$$\int \mathrm{d}\phi g(\phi) \sin\phi = -g(\phi)\cos\phi + \int \mathrm{d}\phi \frac{\mathrm{d}g}{\mathrm{d}\phi} \cos\phi, \tag{29}$$

$$\int \mathrm{d}\phi g(\phi) \cos\phi = g(\phi)\sin\phi - \int \mathrm{d}\phi \frac{\mathrm{d}g}{\mathrm{d}\phi} \sin\phi. \tag{30}$$

SVEA basically means neglecting the second terms containing the derivative of the pulse shape $\mathrm{d}g/\,\mathrm{d}\phi$ because it is $\mathcal{O}(1/\sigma)$ smaller than the first term. For f_2 ($\propto g^2$, cf. Eq. (23)) we use

$$\int \mathrm{d}\phi g^2(\phi)\cos^2\phi \approx \frac{1}{2}\int \mathrm{d}\phi g^2(\phi) + \frac{1}{2}g^2(\phi)\sin\phi\cos\phi, \tag{31}$$

$$\int \mathrm{d}\phi g^2(\phi)\sin^2\phi \approx \frac{1}{2}\int \mathrm{d}\phi g^2(\phi) - \frac{1}{2}g^2(\phi)\sin\phi\cos\phi, \tag{32}$$

which becomes particularly handy if $\int \mathrm{d}\phi\, g^2$ is known analytically, such as for the *sech* pulse (8), where $\int \mathrm{d}\phi \cosh^{-2}\phi/\sigma = \sigma\tanh(\phi/\sigma) + const$, or the Gaussian pulse (9), $\int \mathrm{d}\phi \exp(-\phi^2/2\sigma^2)^2 = \sqrt{\pi}\sigma\mathrm{erf}(\phi/\sigma)/2 + const$, where $\mathrm{erf}(x)$ is the normalized error function. Finally, the SVEA result for the phase reads

$$f_1 = \frac{ma_0}{k\cdot p}g(x_+)\left[p\cdot\epsilon_1\cos\xi\sin\omega x_+ - p\cdot\epsilon_2\sin\xi\cos\omega x_+\right], \tag{33}$$

$$f_2 = -\frac{m^2a_0^2}{4k\cdot p}\left[\int^{\omega x_+}\mathrm{d}\phi g^2(\phi) + g^2(x_+)\cos\omega x_+\sin\omega x_+(\cos^2\xi - \sin^2\xi)\right], \tag{34}$$

generalizing the approximation scheme of [40] to linear laser polarization.

Even for short pulses, such as for $\sigma = 5$ meaning that there are about 5 laser oscillations in the pulse, i.e. the pulse length is $\approx 15\,\mathrm{fs}$ for $\lambda = 800\,\mathrm{nm}$, SVEA is quite a good approximation, see Fig. 4 for selected examples.

C. The spectral distribution of scattered photons and the cross section

In the standard formalism, scattering experiments are thought of as constant streams of particles interacting. Consequently, the square of the S matrix contains a factor T which originates from the square of the energy-momentum conservation which is interpreted as $\delta(P_i - P_f)^2 \to \frac{VT}{(2\pi)^4}\delta(P_i - P_f)$, with the volume V and interaction time T which are both put to infinity. On the purpose of rendering this quantity finite, usually the differential rate per unit time and unit volume $\mathrm{d}w_{i\to f} = \frac{|S_{fi}|^2}{VT}\,\mathrm{d}\Pi$ is considered, where $\mathrm{d}\Pi$ denotes the final state phase space. Here, however, the interaction is happening only within a finite time interval. Because of lacking one δ distribution, the square of the S matrix now reads

$$|S_{fi}|^2 = (2\pi)^3 V\delta(\mathbf{p}'_\perp + \mathbf{k}'_\perp - \mathbf{p}_\perp)\delta(p'_+ + k'_+ - p_+)|N_0\mathscr{M}|^2, \tag{35}$$

where the dependence on the interaction time is contained in $\mathscr{M}$ and is finite. Thus, it is not necessary to define a differential rate per unit time. An appropriate observable is the

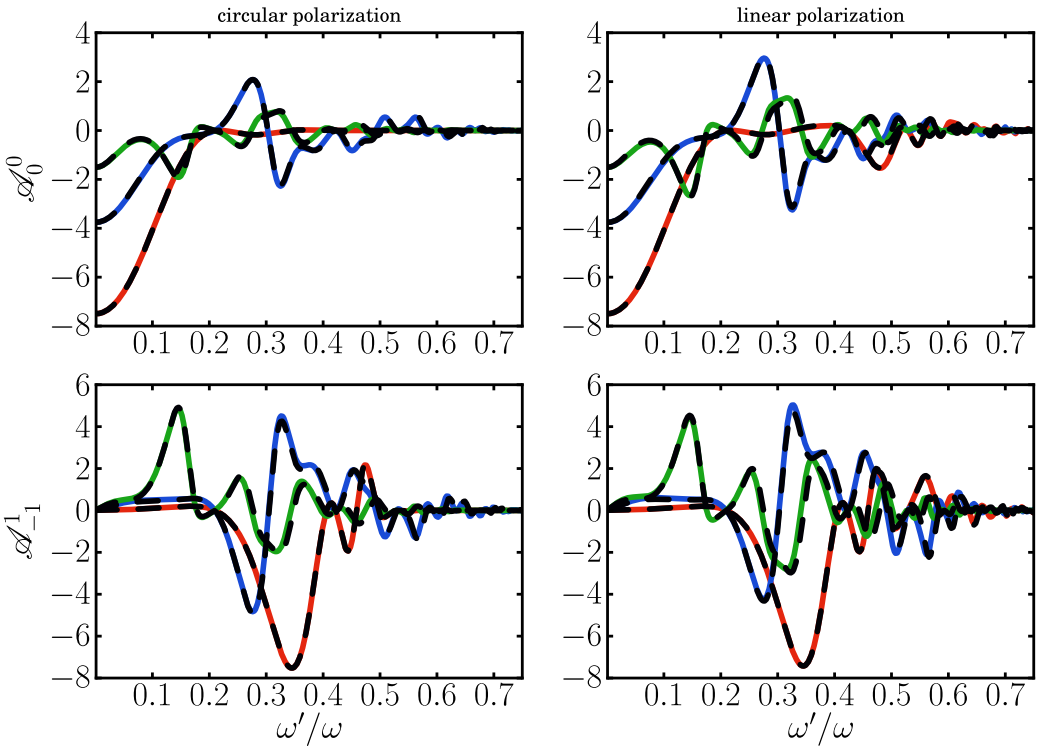

Figure 4. Comparison of the SVEA (black dashed curves) and the full numerical results (solid curves for $\theta = 0$ (red), $\theta = 1/\gamma$ (blue) and $\theta = 2/\gamma$ (green)) for the real parts of the functions $\mathscr{A}_0^0$ and $\mathscr{A}_{-1}^1$ for $\sigma = 5$. Parameters are $a_0 = 1.5$, $\omega = 1.5$ eV, $\gamma = 10^5$. Left (right) panels are for circular (linear) polarization.

emission probability of photons per unit volume and laser pulse

$$\mathrm{d}N = \frac{|S_{fi}|^2}{V}\,\mathrm{d}\Pi, \tag{36}$$

which has as classical analog the spectral density of scattered photons in Thomson scattering (cf. e.g. [26, 37])

$$\frac{\mathrm{d}^2 N_{\mathrm{classical}}}{\mathrm{d}\omega'\,\mathrm{d}\Omega} = -\frac{\omega'}{16\pi^3} j^*(k') \cdot j(k'), \tag{37}$$

$$j^\mu(k') = e \int \mathrm{d}\tau u^\mu(\tau) e^{ik'\cdot x(\tau)}, \tag{38}$$

where $u^\mu(\tau), x^\mu(\tau)$ are the classical velocity and orbit from a solution of the Lorentz force equation for a spinless pointlike charge, and $j^\mu(k')$ is the retarded Fourier transform of the electron current. The notion of Thomson scattering is specified to mean this particular

calculation scheme. A quantum spectral density is given by the Lorentz invariant expression

$$\frac{\mathrm{d}^2 N_{ss'\lambda'}}{\mathrm{d}\omega'\,\mathrm{d}\Omega} = \frac{e^2\omega'}{16\pi^3}\frac{1}{4p_+p'_+}|\mathscr{M}_{ss'\lambda'}|^2, \tag{39}$$

which depends on spin and polarization indices. Averaging over the spin of the incoming electron and summing over the spin of the outgoing electron and the polarization of the outgoing photon yields a quantity which is directly comparable to the classical spectral density

$$\frac{\mathrm{d}^2 N_{\mathrm{quantum}}}{\mathrm{d}\omega'\,\mathrm{d}\Omega} = \frac{1}{2}\sum_{s,s'=1}^{2}\sum_{\lambda'}\frac{\mathrm{d}^2 N_{ss'\lambda'}}{\mathrm{d}\omega'\,\mathrm{d}\Omega}. \tag{40}$$

Now we construct an invariant cross section by dividing Eq. (40) by the normalized number of photons N_L in the laser pulse, i.e.

$$\frac{\mathrm{d}^2\sigma}{\mathrm{d}\omega'\,\mathrm{d}\Omega} = \frac{1}{N_L}\frac{\mathrm{d}^2 N_{\mathrm{quantum}}}{\mathrm{d}\omega'\,\mathrm{d}\Omega} \tag{41}$$

with $N_L = \int_{-\infty}^{\infty}\mathrm{d}t\frac{\langle|\mathbf{S}|\rangle}{\omega}$, where $\mathbf{S} = \mathbf{E}\times\mathbf{B}$ is the Poynting vector of the laser field, derived from the vector potential (7), yielding

$$N_L = \frac{\omega}{2}\frac{a_0^2 m^2}{e^2}\int_{-\infty}^{\infty}\mathrm{d}t\, g(t)^2 \tag{42}$$

with $\int_{-\infty}^{\infty}\mathrm{d}t\cosh^{-2}\phi/\sigma = 2\sigma/\omega$ and $\int_{-\infty}^{\infty}\mathrm{d}t\exp\left(-\phi^2/2\sigma^2\right)^2 = \sqrt{\pi}\sigma/\omega$ for the pulse shapes (8) and (9), respectively. Using this definition, the total cross section is independent of the pulse shape function g and the pulse length σ. (A different definition of the cross section without this property has been proposed in [41].) This has been checked numerically for $a_0 \to 0$ by a comparison of $\frac{\mathrm{d}\sigma}{\mathrm{d}\Omega} = \int\mathrm{d}\omega'\frac{\mathrm{d}^2\sigma}{\mathrm{d}\omega'\,\mathrm{d}\Omega}$ with the differential Klein-Nishina cross section [48], or σ_{tot} with the total Klein-Nishina cross section. In particular, in the limit $y_1 \to 0$ we obtain the total Thomson cross section $\sigma_T = 665.25$ mb accurately, as exhibited in Fig. 5 for three different pulse shapes and pulse lengths.

IV. DISCUSSION

A. Monochromatic Limit

In the famous case of monochromatic Compton scattering, the frequency of the scattered photon is uniquely defined by the scattering angle. For a finite temporal laser pulse, however,

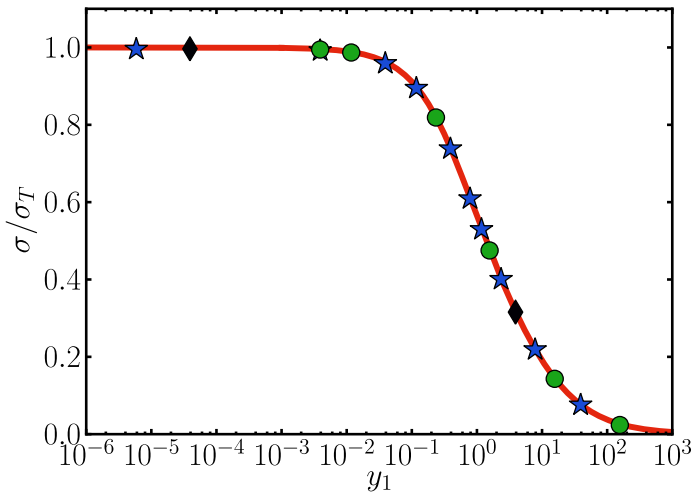

Figure 5. Total cross section for Compton scattering normalized to the Thomson cross section σ_T. Red curve: Klein-Nishina cross section. Symbols: numerically calculated cross section in a pulsed laser field with $a_0 = 0.001$. Blue stars: $\sigma = 20$ for a *cosh* pulse; green circles: $\sigma = 30$ for a Gaussian pulse; black diamonds: $\sigma = 100$ for a Gaussian pulse.

this tight relation is lost. As outlined in subsection III C, there is a distribution of the emitted photons for a fixed angle. As an example, we exhibit in the left top panel of Fig. 6, the spectral density $\mathrm{d}^2N/\,\mathrm{d}\omega'\,\mathrm{d}\Omega$ as a function of $\varpi' = \omega'/\omega'_{1,\mathrm{classical}}$ for fixed Ω. The vertical thin lines depict the positions of the harmonics for a monochromatic plane wave with infinite duration and the same value of a_0, given by [48]

$$\omega'_\ell = \omega'_{\ell,\mathrm{quantum}} = \frac{\ell k\cdot q}{(q+\ell k)\cdot n'}, \tag{43}$$

introducing the intensity dependent quasi-momentum of the electron $q_-^{(\prime)} = p_-^{(\prime)} + b_{p^{(\prime)}}k_-$ with $b_{p^{(\prime)}} = m^2a_0^2/4k\cdot p^{(\prime)}$ and the dressed mass-shell relation $q^2 = q'^2 = m_*^2 = m^2(1+a_0^2/2)$. Note that only $p_-^{(\prime)}$, the conjugate momentum to x_+, is modified by an intensity dependent contribution, i.e. $q_+^{(\prime)} = p_+^{(\prime)}$ and $\mathbf{q}_\perp^{(\prime)} = \mathbf{p}_\perp^{(\prime)}$. The integer ℓ labels the individual harmonics, which are not equidistant in general.

In a pulsed laser field, each harmonic consists of a bunch of spectral "lines" (or subpeaks) visible in the top panels of Fig. 6 with a certain width $\Delta\omega'_\ell$ determined by the minimum and maximum values of intensity in the laser pulse. The high-energy tail of each harmonic bunch is given by $\omega'_\ell(a_0 \to 0)$, and is produced at the edges of the laser pulse. The low-energy edge is given by $\omega'_\ell(a_0)$ and accounts for the maximum red-shift at the center of the pulse. Thus,

the spectral width of each harmonic ℓ is given by

$$\begin{aligned}\Delta\omega'_\ell &= \omega'_\ell(a_0 \to 0) - \omega'_\ell(a_0) \\ &= \omega'_\ell(a_0)\omega'_\ell(a_0 \to 0)\frac{b_p k\cdot n'}{\ell k\cdot p}.\end{aligned} \tag{44}$$

The number of subpeaks in a bunch is proportional to the pulse length σ and the intensity a_0^2. The highest subpeak takes its maximum value at a higher frequency ω' than predicted by (43), thus, at a smaller intensity-dependent red-shift than the monochromatic harmonics due to a lower average a_0. Hence, one could say that this maximum is blue-shifted as compared to the monochromatic plane wave.

Increasing σ from 20 to 50 does not lead to an accumulation of spectral weight at the non-linear Compton frequencies as could be expected naively. The number of subpeaks increases but the average shape of the harmonic bunch is more or less the same for $\sigma = 20$ and 50 with the same spectral width. In fact, to obtain the monochromatic limit, it is not efficient to take simply the limit $\sigma \to \infty$. A method with better convergence is to introduce a flat-top area in the pulse. This however, introduces a second pulse length parameter: The total pulse length now consists of the rise "time" σ and the flat-top "time" τ. The flat-top part of the pulse is parametrized as $g_{\text{flat}}(\phi) = \Theta(\phi + \pi\tau)\Theta(\pi\tau - \phi)$, where a factor π is introduced so that τ is comparable to the Gaussian and *cosh* widths σ in terms of laser oscillations under the envelope, and $\Theta(\phi)$ is the Heaviside step function. Then, the complete pulse is parametrized as

$$g_{\text{tot}}(\phi;\sigma,\tau) = \Theta(\phi+\pi\tau)\Theta(\pi\tau-\phi) + g(\phi-\pi\tau)\Theta(\phi-\pi\tau) + g(\phi+\pi\tau)\Theta(-\phi-\pi\tau). \tag{45}$$

The spectrum converges rather fast to sharp peaks centered at the non-linear Compton frequencies upon increasing τ from 0 to 30 while keeping $\sigma = 20$ constant, as seen in the bottom panel of Fig. 6: The strengths are located at the sharp non-linear Compton energies. The remaining wiggles around the non-linear Compton energies vanish upon increasing τ further.

In the monochromatic limit $\tau \to \infty$, the rising and trailing edges of the pulse shape function become unimportant, i.e. $g \to 1$, and the function H_+ in (24) reduces to

$$\begin{aligned}H_+ = {} & \tfrac{1}{2}(k'_- + q'_- - q_-)x_+ + \alpha_1 \sin\omega x_+ - \alpha_2\cos\omega x_+ \\ & -\tfrac{b_p - b_{p'}}{2}(\cos^2\xi - \sin^2\xi)\sin 2\omega x_+\end{aligned} \tag{46}$$

with $\alpha_i = ma_0(\epsilon_i\cdot p/k\cdot p - \epsilon_i\cdot p'/k\cdot p')$ and re-identifying the electron quasi-momenta $q_-^{(\prime)}$. Upon plugging (46) into (15) and expanding into a Fourier series, one obtains a fourth

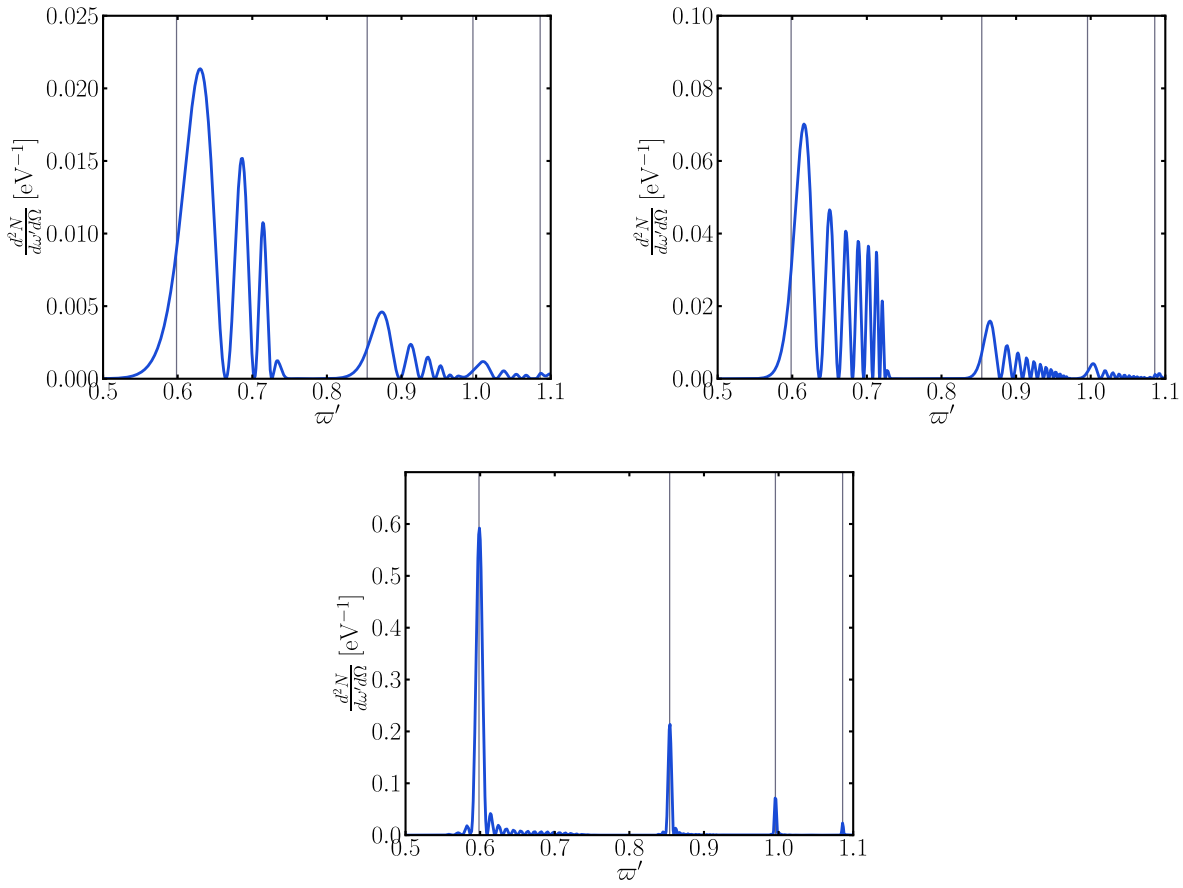

Figure 6. Top panels: Spectral density $\mathrm{d}^2N/\,\mathrm{d}\omega'\,\mathrm{d}\Omega$ as a function of the scaled frequency $\varpi' = \omega'/\omega'_{1,\mathrm{classical}}$ for a *cosh* pulse with $\sigma = 20$ (left) and 50 (right). Bottom panel: Spectral density for a flat-top pulse with *cosh* edges, $\tau = 30$ and $\sigma = 20$. In all panels $a_0 = 1.0$, $\gamma = 10^5$, $\omega = 1.5$ eV, $\theta = 1/\gamma$ and $\varphi = 0$. The thin vertical lines depict the non-linear Compton energies defined in Eq. (43).

energy-momentum conservation by integrating over x_+, yielding $q_- + \ell k_- = q'_- + k'_-$. The four energy-momentum constraints together lead again to Eq. (43).

The individual harmonics, consisting of a multitude of subpeaks, begin to overlap if the lower edge of the $\ell + 1$st harmonic coincides with the upper edge of the ℓth harmonic, i.e.

$$\omega'_\ell(a_0 \to 0) \geq \omega'_{\ell+1}(a_0). \tag{47}$$

This happens always for sufficiently large values of a_0 and ℓ. The notion of individual harmonics becomes inappropriate, as one rather observes a continuous spectral distribution.

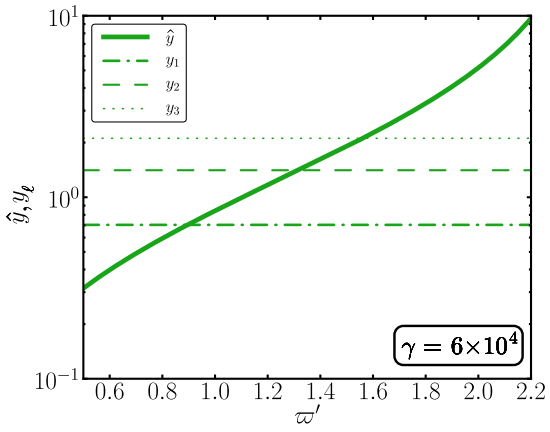

Figure 7. Different recoil parameters $\hat{y}(\omega')$ and y_ℓ for $\ell = 1, 2, 3$ as a function of the scaled frequency $\varpi' = \omega'/\omega'_{1,\text{classical}}$.

B. Comparison with Thomson scattering

There are different bookkeeping parameters for the characterization of the Thomson regime as limiting case of the presently considered scenario. One parameter is y_ℓ introduced in Eq. (2). An alternative would be to employ the outgoing momenta instead of the incoming ones, defining $\hat{y} = (\hat{s} - m^2)/m^2$ with $\hat{s} = (p' + k')^2$. When four-momentum conservation holds, both definitions coincide (since k' and p' both depend on ℓ) and $\hat{s}$ coincides with the usual Mandelstam variable s. However, this is not the case here. These recoil parameters are compared in Fig. 7. The parameter $\hat{y}$ is a function of ω', as it depends on ω' through k'

$$\hat{y} = 2\frac{p'\cdot k'}{m^2} = \frac{2}{m^2}\frac{(p\cdot k')\,(p\cdot k)}{(p\cdot k - k'\cdot k)} = \frac{2\gamma^2\omega'(1-\mathbf{n}'\cdot\boldsymbol{\beta})}{m\gamma - \omega'\frac{1-\mathbf{n}\cdot\mathbf{n}'}{1-\mathbf{n}\cdot\boldsymbol{\beta}}}, \tag{48}$$

which diverges at $\omega'_\infty = \frac{m\gamma(1-\mathbf{n}\cdot\boldsymbol{\beta})}{1-\mathbf{n}\cdot\mathbf{n}'}$, defining the boundary of phase space. Thus the physical phase space is given by $0 \le \theta < \pi$, $0 \le \varphi < 2\pi$ and $0 < \omega' < \omega'_\infty$. An interpretation of the phase space boundary will be given in subsection IV C.

To relate the Compton amplitude with the classical Thomson counterpart it is instructive to consider the phase exponential, e.g. $H_+ \pm \omega x_+$ in $\mathscr{A}^1_{\pm 1}$, cf. Eq. (25). For the sake of simplicity, a backscattering head-on geometry with a circularly polarized laser is assumed

in this subsection. Then, after using some light-cone algebra, the phase reads

$$H_+ \pm \omega x_+ = \left[(k'_- + p'_- - p_-) \pm \omega\right] x_+ - \left(\frac{m^2 a_0^2}{2k\cdot p} - \frac{m^2 a_0^2}{2k\cdot p'}\right) \int^{\omega x_+} \mathrm{d}\phi\, g^2(\phi) \tag{49}$$

$$= \left[\frac{k'\cdot p}{n_+\cdot p'} \pm \omega\right] x_+ + \frac{k'\cdot k}{(k\cdot p)(k\cdot p')}\frac{m^2 a_0^2}{2} \int^{\omega x_+} \mathrm{d}\phi\, g^2(\phi). \tag{50}$$

Momentum conservation implies $n_+\cdot p' = n_+\cdot p - n_+\cdot k'$ (see (A7)). For $n_+\cdot k' \ll n_+\cdot p$, the leading term

$$\left[\frac{k'\cdot p}{n_+\cdot p} x_+ \pm \omega\right] + \frac{k'\cdot k}{(k\cdot p)^2}\frac{m^2 a_0^2}{2} \int^{\omega x_+} \mathrm{d}\phi\, g^2(\phi) = k'\cdot x(\tau) \pm \omega x_+ \tag{51}$$

agrees with the corresponding expression obtained in a classical calculation for Thomson scattering (cf. [37], see also Eq. (38)). The frequency of back-scattered photons in monochromatic plane waves is obtained from (43) by neglecting ℓk w.r.t. q in the denominator, i.e.

$$\omega'_{\ell,\mathrm{classical}} = \ell \frac{k\cdot q}{q\cdot n'}. \tag{52}$$

In Thomson scattering, the harmonics are always equidistant. A series of plots showing the transition from Thomson to Compton scattering is exhibited in Fig. 8. The deviations between Thomson and Compton scattering are: (i) a non-linear red-shift in frequency and (ii) a slight modification in the amplitude starting notably at $y_1 = 0.12$. It is obvious that the red-shift is much more pronounced at higher frequencies. Figure 8 quantifies the well known fact [48] that Compton scattering turns into Thomson scattering in the low-energy limit. For the chosen parameters ($a_0 = 1.0, \omega = 1.5$ eV) the differences become significant for $\gamma \geq 10^4$. Very drastic differences are obvious for $\gamma = 10^5$ (bottom right panel of Fig. 8).

C. Scaling properties of the spectral density

The classical and quantum spectral densities for arbitrary pulse shapes are connected by the scaling law

$$\frac{\mathrm{d}^2 N_{\mathrm{classical}}}{\mathrm{d}\omega'\,\mathrm{d}\Omega}(\omega',\theta) = \eta \frac{\mathrm{d}^2 N_{\mathrm{quantum}}}{\mathrm{d}\omega'\,\mathrm{d}\Omega}(\chi\omega',\theta) \tag{53}$$

with the two scaling factors η and χ which are determined by the monochromatic results. The frequency scaling factor χ is given by

$$\chi = \frac{\omega'_{\ell,\mathrm{quantum}}}{\omega'_{\ell,\mathrm{classical}}} = \frac{n'\cdot u + n'\cdot n\frac{a_0^2}{4n\cdot u}}{n'\cdot u + n'\cdot n\left(\frac{a_0^2}{4n\cdot u} + \ell\frac{\omega}{m}\right)} = \frac{q\cdot n'}{(q+\ell k)\cdot n'}. \tag{54}$$

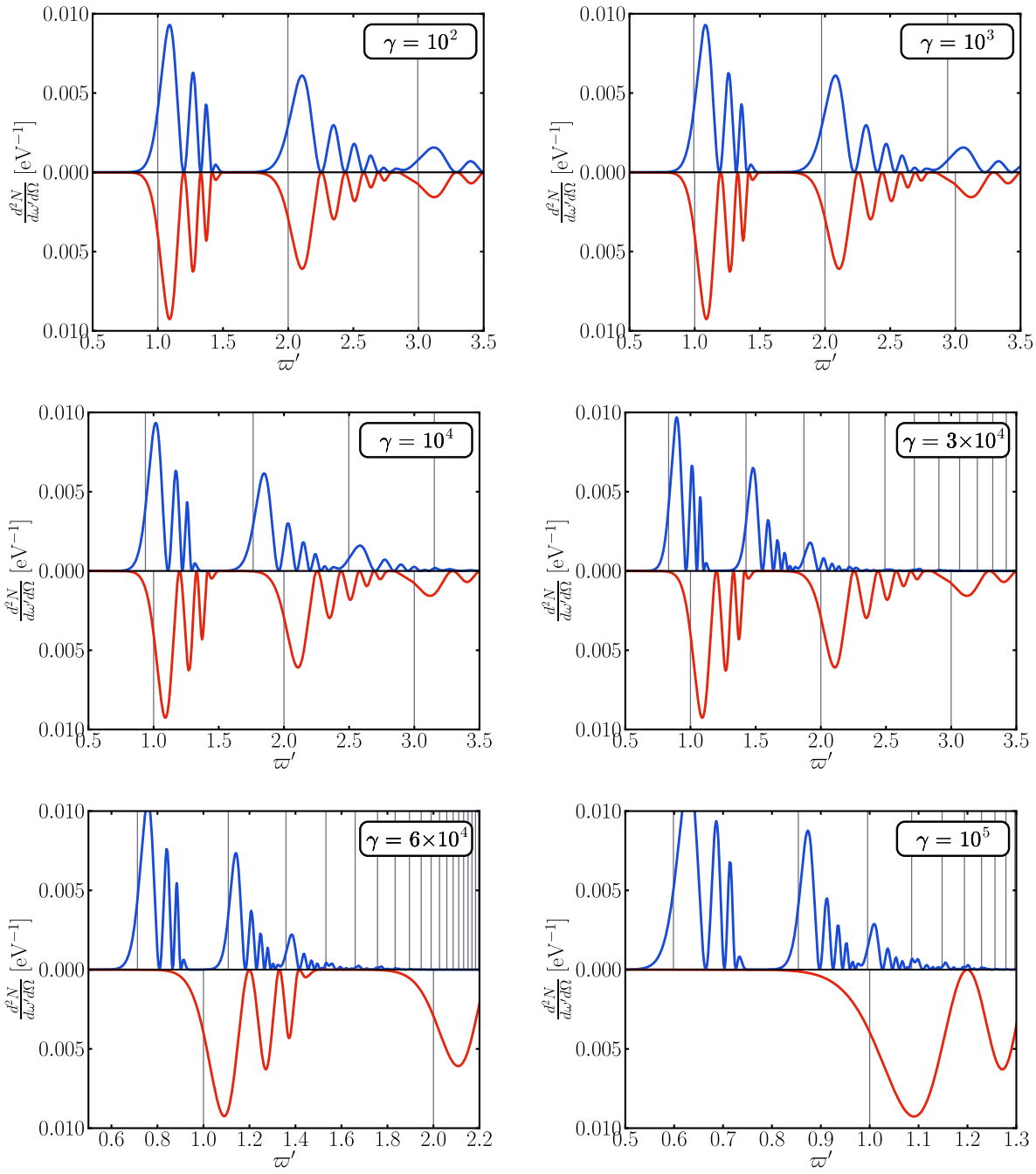

Figure 8. The photon spectrum as a function of the scaled frequency $\varpi' = \omega'/\omega'_{1,\mathrm{classical}}(\theta)$ for $\gamma = 10^2, 10^3, 10^4, 3\times10^4, 6\times10^4, 10^5$ (i.e. $y_1 = 0.0012, 0.012, 0.12, 0.35, 0.7, 1.2$) from top left to bottom right for $\theta = 1/2\gamma$ and $\varphi = 0$ for a *cosh* pulse shape. The upper (lower) blue (red) curves are for a quantum (classical) calculation of Compton (Thomson) scattering. The vertical gray lines mark the positions of the monochromatic harmonics Eqs. (43) and (52), respectively. The other parameters are $a_0 = 1.0$, $\omega = 1.5$ eV, $\sigma = 20$ and $\xi = 0$, i.e. linear laser polarization.

A continuous effective ℓ_{eff} has to be used, which follows from the inversion of $\omega'_{\ell,\text{quantum}}$, yielding

$$\ell_{\text{eff}}(\omega') = \frac{\frac{\omega'}{\omega}\left(n'\cdot u + n'\cdot n\frac{a_0^2}{4n\cdot u}\right)}{n\cdot u - n'\cdot n\frac{\omega'}{m}} = \frac{q\cdot k'}{q\cdot k - k'\cdot k}, \tag{55}$$

which simplifies to $\chi = 1 - k'\cdot k/p\cdot k = 1 - k'_+/p_+$. The scaling of the frequency naturally also includes the scaling behavior of the phase space factor which is proportional to ω'^2. The scaling factor η describes the scaling of the differential probabilities defined by

$$\eta = \left(\omega'^{-2}_{\text{quantum}}\frac{\mathrm{d}\sigma_{\text{quantum}}}{\mathrm{d}\Omega}\right)\left(\omega'^{-2}_{\text{classical}}\frac{\mathrm{d}\sigma_{\text{classical}}}{\mathrm{d}\Omega}\right)^{-1}, \tag{56}$$

where the differential cross sections $\mathrm{d}\sigma_{\text{quantum}}$ and $\mathrm{d}\sigma_{\text{classical}}$ are the monochromatic plane-wave cross sections, yielding for circular polarization [37]

$$\eta = \frac{\mathfrak{J}_\ell}{\mathfrak{K}_\ell} = 1 + \frac{x^2}{1+x}\frac{\mathfrak{L}_\ell}{2\mathfrak{L}_\ell - \frac{8}{a_0^2}J_\ell^2(z)}, \tag{57}$$

where $x = (1-\chi)/\chi$, $y_* = 2\ell k\cdot p/m_*^2$ and ℓ_{eff} has to be used instead of ℓ everywhere. The other definitions are $\mathfrak{L}_\ell = J_{\ell+1}^2(z) + J_{\ell-1}^2(z) - 2J_\ell^2(z)$, $\mathfrak{K}_\ell = -8J_\ell^2(z)/a_0^2 + 2\mathfrak{L}_\ell$, $\mathfrak{J}_\ell = \mathfrak{K}_\ell + \frac{x^2}{1+x}\mathfrak{L}_\ell$ and $z = 2\ell\sqrt{\frac{a_0^2/2}{1+a_0^2/2}}\sqrt{\frac{x}{y_*}(1-\frac{x}{y_*})}$; J_ℓ are Bessel functions of the first kind. In the limit $a_0 \to 0$ one gets

$$\lim_{a_0\to 0}\eta = 1 + \frac{x^2}{1+x}\frac{1}{2 - 4\frac{x}{y_*}(1-\frac{x}{y_*})} \tag{58}$$

which is a good approximation for $a_0 < 1$. For linear laser polarization we expect a similar relation to hold, but with the appropriate linearly polarized monochromatic plane-wave cross section instead.

The scaling function χ is related to the momentum transfer from the incoming electron to the outgoing electron via $p'_+ = \chi p_+$. Thus, χ is the fraction of p_+ momentum transferred from the incoming electron to the outgoing electron p'_+. Furthermore, the fraction of momentum transferred to the photon is $k'_+ = (1-\chi)p_+$ thus, $1-\chi$ is another measure of the electron recoil. χ is a monotonic decreasing function of ω'. The point $\chi(\omega') = 0$ corresponds to $p'_+ = 0$ and $k'_+ = p_+$, i.e. the total amount of momentum is transferred from the electron to the photon. Further increasing ω' would render χ as well as p'_+ negative. This defines the boundary of the physical phase space for the outgoing particles. When $p'_+ < 0$, then, due to the free particle dispersion relation (A6), also $p'_- < 0$. This, however, would lead to a

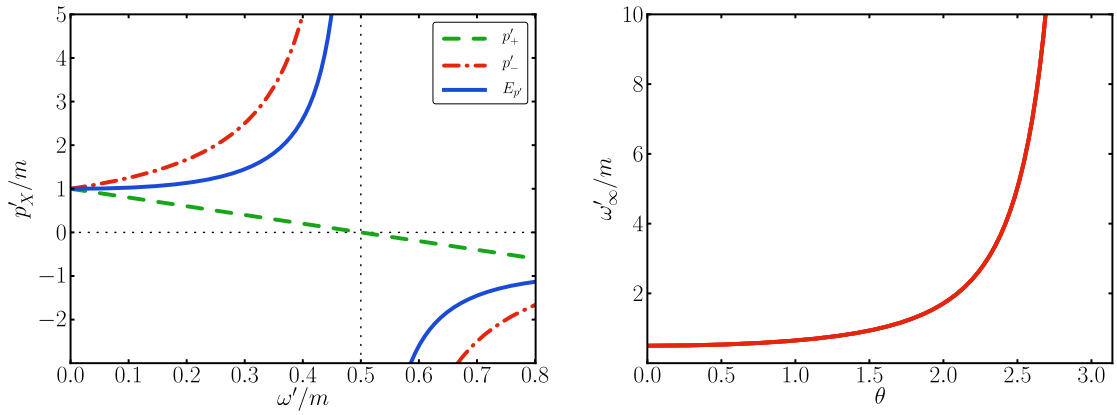

Figure 9. Left panel: Different components of the outgoing electron momentum p'_X as a function of frequency ω' for backscattering geometry in the rest frame of the incoming electron. Shown are p'_- (red, dash-dotted), p'_+ (green, dashed) and $p'_0 = E_{p'}$ (blue, solid). The physical phase space has its support at $\chi > 0$, i.e. for $0 < \omega'/m < 0.5 = \omega'_\infty/m$ in this case. Right panel: Maximum frequency ω'_∞ as function of scattering angle θ, where $\theta = 0$ denotes the backscattering direction.

negative energy $E_{p'}$ due to $E_{p'} = (p'_+ + p'_-)/2 < 0$. Consequently, there exists a maximum frequency ω'_∞, defined by $\chi(\omega'_\infty) = 0$:

$$\omega'_\infty = \frac{p \cdot k}{n' \cdot k} = \frac{m\gamma(1 - \mathbf{n} \cdot \boldsymbol{\beta})}{1 - \mathbf{n} \cdot \mathbf{n}'}, \tag{59}$$

which can also be obtained as the limit $\lim_{\ell \to \infty} \omega'_\ell = \omega'_\infty$, with ω'_ℓ from Eq. (43). This also coincides with the singularity in $\hat{y}$, see Eq. (48). For the backscattering head-on geometry we obtain $\omega'_\infty = m/2$ for electrons initially at rest and $\omega'_\infty = m\gamma(1 + \beta)/2 \approx E_p$ for ultrarelativistic particles, i.e. the maximum backscattered frequency is determined by the energy of the incoming electron. The momentum components p'_+, p'_- and $E_{p'}$ are depicted in the left panel of Fig. 9 as a function of ω' in the electron rest frame. The right panel of Fig. 9 shows the dependence of ω'_∞ on the scattering angle θ. It takes its minimum at the backscattering direction $\theta = 0$ and goes to infinity in the limit $\theta \to \pi$, i.e. forward scattering.

D. Further differences between the classical and QED calculations

As demonstrated in the preceding subsections and quantified by the scaling law, the main difference between the spectral densities of Thomson and Compton scattering is the proper treatment of the electron recoil in the latter one. Additionally, there is another regime where

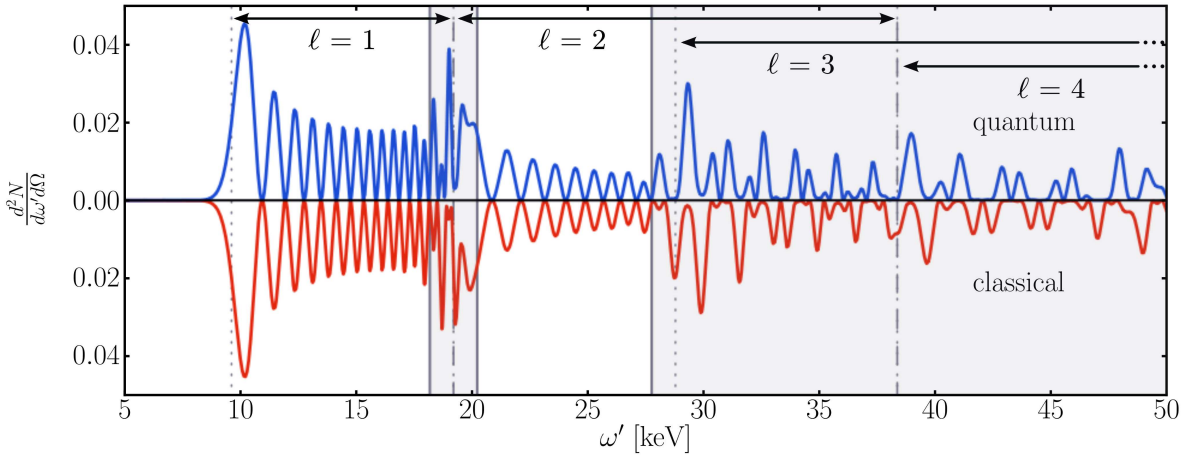

Figure 10. Comparison of the quantum (upper) and classical (lower) spectral distributions $\mathrm{d}^2N/\,\mathrm{d}\omega'\,\mathrm{d}\Omega$ as a function of ω' for fixed angles $\theta = 1/\gamma$, $\varphi = 0$. The overlap regions of different "harmonics" are highlighted as gray shaded areas. Parameters are $\sigma = 50$, $\omega = 1.5$ eV, $a_0 = 2.0$, $\gamma = 80$, i.e. $\hat{y} \leq 2.5 \times 10^{-3}$.

the quantum description goes beyond a classical calculation, even if $\hat{y} \ll 1$, where the total Thomson and Compton cross sections are equal in leading order. This happens in regions of phase space where individual harmonics are overlapping (see Eq. (47)). There, the subpeaks in the quantum calculation show completely different patterns in comparison to a classical calculation, see Fig. 10. Consequently, the scaling law may not be applied where harmonics are overlapping. For a better orientation, the spectral ranges of the individual harmonics are marked in Fig. 10, where the lower (upper) edges are depicted by dotted (dashed) lines. Due to the finite pulse length σ, the actual spectral distribution reaches over these edges by $\mathcal{O}(\tilde{\sigma})$, where $\tilde{\sigma} = \gamma^2(1+\beta)^2/\sigma$. The gray shaded areas mark the overlapping regions with a width of $2\tilde{\sigma}$.

The generation of the subpeaks can be described as an interference effect [37]. Thus, when the harmonics overlap, for a fixed value of ω' there are contributions from different harmonics and their interference reacts very sensitive to subtle changes in the phase of the $\mathscr{A}_N^M$ functions, see Eqs. (50) and (51). The difference in the spectral distributions looks qualitatively similar to figure 1 of [38], where the influence of classical radiation reaction force on the spectrum was studied. The radiation reaction force also provides an electron recoil in the classical calculation, slightly changing the phases and leading to a modified spectrum.

V. SUMMARY

In this paper, we discussed non-linear Compton scattering in the Furry picture and employed light cone coordinates for temporally shaped laser pulses. We emphasized the structure of the Volkov wavefunctions in a pulsed laser field. We clearly uncovered the modifications of the electron wavefunction due to their interaction with the laser field. The S matrix element for non-linear Compton scattering was evaluated in the framework of Volkov states within the Furry picture. An expression for the cross section which is independent of the pulse shape and pulse length was presented.

We focused on the differences between classical calculations of non-linear Thomson scattering and quantum calculations of non-linear Compton scattering. In both cases, spectral broadening and harmonic substructures have been found, which are, however, shifted in the quantum calculation. These harmonic substructures, still lacking an experimental verification, are interpreted as an interference effect. We found that for $y_\ell \ll 1$ the differential quantum transition probability in many cases coincides with the classical Thomson scattering result also for pulsed laser fields, i.e. quantum effects are mostly negligible in this regime. Also the total Compton cross section coincides with the Thomson cross section σ_T for $y_\ell < 10^{-2}$.

As a main result, we presented a scaling law, connecting the classical and quantum spectral densities for arbitrary y_ℓ, e.g. $y_\ell > 10^{-2}$, relating the classical and quantum results. The remarkable feature is, that the substructures of individual harmonics are also simply scaled. One might speculate that the scaling law may also be applied for arbitrary laser beams, in particular, for strongly focused beams. Hence, it might serve as a tool to add recoil effects to results obtained within classical Thomson scattering models.

Furthermore, we also found regions in phase space, where the differential probabilities for Thomson and Compton are different, although $y_\ell < 10^{-2}$ and the total cross sections coincide. This happens for sufficiently large values of a_0, when the individual harmonics are overlapping. In these regions of phase space, both spectral densities show different, almost erratic behavior. This observation is in qualitative agreement with previous studies of the effect of the radiation reaction force on the spectrum of non-linear Thomson scattering. The radiation reaction force introduces an electron recoil in Thomson scattering to the classical picture. Of course, the scaling law is not applicable in the regions where the spectral

densities show this erratic behavior.

ACKNOWLEDGMENTS

The authors gratefully acknowledge stimulating discussions with T. E. Cowan and K. Chouffani.

Appendix A: Light cone coordinates

1. Basic definitions

The light cone components of a four-vector $x^\mu = (t, x, y, z)$ are defined as $x_\pm, \mathbf{x}_\perp$ by

$$x_- = t - z, \qquad x_+ = t + z, \qquad \mathbf{x}_\perp = (x, y). \tag{A1}$$

In these new coordinates, the scalar product reads $x \cdot y = \frac{1}{2}(x_+ y_- + x_- y_+) - \mathbf{x}_\perp \cdot \mathbf{y}_\perp$. Arranging these components as a four-vector $X^\mu = (x_+, x_-, \mathbf{x}_\perp)$, one may introduce a non-diagonal metric

$$g_{\mu\nu} = \begin{pmatrix} 0 & \frac{1}{2} & 0 & 0 \\ \frac{1}{2} & 0 & 0 & 0 \\ 0 & 0 & -1 & 0 \\ 0 & 0 & 0 & -1 \end{pmatrix} \tag{A2}$$

with $\sqrt{-g} = 1/2$, thus $\mathrm{d}^4x \to \frac{1}{2}\,\mathrm{d}x_+\,\mathrm{d}x_-\,\mathrm{d}^2\mathbf{x}_\perp$. The inverse transformation is given by $x_0 = \frac{1}{2}(x_+ + x_-),\ x_3 = \frac{1}{2}(x_+ - x_-)$.

More generally, light cone coordinates can be introduced by projecting onto a light-like four-vector, which is in our case given by the laser wave vector $k^\mu = \omega n_+^\mu = \omega(1, \mathbf{n})$ defining a direction $\mathbf{n}$ with $\mathbf{n} \cdot \mathbf{n} = 1$. The coordinate system will always be aligned such that $\mathbf{n} = (0, 0, -1)$. Then the light cone components of a vector B^μ may be defined by projection via

$$B_+ = B \cdot n_+, \quad B_- = B \cdot n_-, \tag{A3}$$

$$\mathbf{B}_\perp = \mathbf{B} - (\mathbf{B} \cdot \mathbf{n})\mathbf{n} \tag{A4}$$

with $n_-^\mu = (1, -\mathbf{n})$. Additionally, we need the orthonormal transverse basis vectors $\epsilon_i, i = (1, 2)$ with $\epsilon_i \cdot n_\pm = 0$ and $\epsilon_i \cdot \epsilon_j = -\delta_{ij}$, i.e. the transverse part of B^μ may also be defined as $\mathbf{B}_\perp = (B_1, B_2),\ B_i = B \cdot \epsilon_i$. With this convention of light cone coordinates, the conjugate momentum to x_+ is P_- and vice versa.

2. Kinematics in light cone coordinates

Special light cone coordinates may be defined with respect to the laser momentum $k^\mu = \omega(1, \mathbf{n})$ with $\mathbf{n} = -\mathbf{e}_z$. Let be the momentum of the incoming electron $p^\mu = (E_p, \mathbf{p}) =$

$m\gamma(1,\boldsymbol{\beta}) = mu^\mu$ with $\boldsymbol{\beta} = -\beta\mathbf{n}$ and the momentum of the outgoing photon $k'^\mu = (\omega', \mathbf{k}') = \omega'(1,\mathbf{n}') = \omega' n'^\mu$ with $\mathbf{n}' = (\cos\varphi\sin\theta, \sin\varphi\sin\theta, \cos\theta)$. Then the light cone components of these vectors read

$$\begin{aligned} k_- &= 2\omega, & k_+ &= 0, & \mathbf{k}_\perp &= 0, \\ k'_- &= \omega'(1+\cos\theta), & k'_+ &= \omega'(1-\cos\theta), & \mathbf{k}'_\perp &= \omega'\sin\theta(\cos\varphi, \sin\varphi), \\ p_- &= m\gamma(1-\beta), & p_+ &= m\gamma(1+\beta), & \mathbf{p}_\perp &= 0. \end{aligned} \tag{A5}$$

The free particle dispersion relation $E_p^2 = \mathbf{p}^2 + m^2$ reads in light cone coordinates

$$p_- = \frac{\mathbf{p}_\perp^2 + m^2}{p_+}. \tag{A6}$$

Using momentum conservation, one obtains for the components of p'

$$\begin{aligned} \mathbf{p'}_\perp &= \mathbf{p}_\perp - \mathbf{k}'_\perp, \\ p'_+ &= p_+ - k'_+. \end{aligned} \tag{A7}$$

It is worth noting that there is in general no conservation law for the component p'_-. That component is fixed by the dispersion relation (A6) yielding

$$p'_- = \frac{m^2 + (p'_\perp)^2}{p'_+} = \frac{m^2 + (\mathbf{p}_\perp - \mathbf{k}_\perp{}')^2}{p_+ - k'_+}. \tag{A8}$$

All the components of p' have to be considered as a function of ω' and $\mathbf{n}'$. The projection of p' onto k may be rewritten as

$$k \cdot p' = k_- p'_+ = k_-(p_+ - k'_+) = k\cdot p - k\cdot k', \tag{A9}$$

from which the important relation

$$\frac{1}{k\cdot p} - \frac{1}{k\cdot p'} = -\frac{k\cdot k'}{k\cdot p\; k\cdot p'} \tag{A10}$$

may be derived. Eventually, we present a useful collection of relations between momentum components:

$$k'_- + p'_- - p_- = \frac{2p\cdot k'}{p'_+} = 2\frac{p\cdot k'}{p'\cdot k}, \tag{A11}$$

$$y = \frac{2p'\cdot k'}{m^2} = \frac{p_+(k'_- + p'_- - p_-)}{m^2} = \frac{p_+}{p'_+}\frac{2p\cdot k'}{m^2}, \tag{A12}$$

$$\frac{p'\cdot k'}{p\cdot k'} = \frac{p_+}{p'_+} = \frac{p\cdot k}{p'\cdot k}, \tag{A13}$$

$$\chi = 1 - \frac{k'\cdot k}{p\cdot k} = \frac{p\cdot k'}{p'\cdot k'}. \tag{A14}$$

Appendix B: Fourier expansion of the Volkov wavefunction

Here, we provide a Fourier expansion of the Volkov state (5) in a pulsed laser field to gain further insight to the structure of the Volkov state and to use it as an alternative way to obtain the matrix element for non-linear Compton scattering as a convolution in momentum space. We define the Fourier transformations in x_-, x_+ and $\mathbf{x}_\perp$ directions with different signs according to the metric (A2)

$$\begin{aligned}\tilde{F}(\mathbf{Q}_\perp, Q_+, Q_-) &= \tfrac{1}{2}\int \mathrm{d}^2\mathbf{x}_\perp\, \mathrm{d}x_-\, \mathrm{d}x_+ F(\mathbf{x}_\perp, x_-, x_+) e^{\frac{i}{2}(Q_- x_+ + Q_+ x_-) - i\mathbf{Q}_\perp\cdot\mathbf{x}_\perp},\\ F(\mathbf{x}_\perp, x_-, x_+) &= \tfrac{1}{2}\int \tfrac{\mathrm{d}^2\mathbf{Q}_\perp\, \mathrm{d}Q_+\, \mathrm{d}Q_-}{(2\pi)^4} \tilde{F}(\mathbf{Q}_\perp, Q_+, Q_-) e^{-\frac{i}{2}(Q_- x_+ + Q_+ x_-) + i\mathbf{Q}_\perp\cdot\mathbf{x}_\perp}.\end{aligned} \tag{B1}$$

The Fourier transform of the Volkov matrix $C_p(x)$ (see Eq. (11)) reads

$$\begin{aligned}\tilde{C}_p(\mathbf{Q}_\perp, Q_+, Q_-) \;=\; & (2\pi)^3\delta^2(\mathbf{Q}_\perp - \mathbf{p}_\perp)\delta(Q_+ - p_+)\\ & \times\Big\{\mathscr{G}_0(Q_-) + d_p \not{k}\big[\not{\epsilon}_- \mathscr{G}_1(Q_-) + \not{\epsilon}_+ \mathscr{G}_{-1}(Q_-)\big]\Big\}\end{aligned} \tag{B2}$$

with

$$\mathscr{G}_N(Q_-) = \int \mathrm{d}x_+ e^{\frac{i}{2}(Q_- - p_-)x_+} g^{|N|}(x_+) e^{iN\omega x_+ + if(x_+)}. \tag{B3}$$

The functions $\mathscr{G}_N$ describe the nontrivial, pulse dependent momentum distribution of the Volkov wavefunction. Using the Fourier representation of the Volkov state, the matrix element for non-linear Compton scattering (13) reads

$$\begin{aligned}S_{fi} \;=\; & N_0(2\pi)^3\delta^2(\mathbf{p}'_\perp + \mathbf{k}'_\perp - \mathbf{p}_\perp)\delta(p'_+ + k'_+ - p_+)\times\\ & \times\Big[\mathscr{T}^0_0(\mathscr{G}^*_0 \star \mathscr{G}_0) + \mathscr{T}^1_{-1}(\mathscr{G}^*_0 \star \mathscr{G}_1 + \mathscr{G}^*_{-1} \star \mathscr{G}_0)\\ & + \mathscr{T}^1_1(\mathscr{G}^*_0 \star \mathscr{G}_{-1} + \mathscr{G}^*_1 \star \mathscr{G}_0) + \mathscr{T}^2_0(\mathscr{G}^*_1 \star \mathscr{G}_1 + \mathscr{G}^*_{-1} \star \mathscr{G}_{-1})\\ & + \mathscr{T}^2_{-2}(\mathscr{G}^*_{-1} \star \mathscr{G}_1) + \mathscr{T}^2_2(\mathscr{G}^*_1 \star \mathscr{G}_{-1})\Big]\end{aligned} \tag{B4}$$

with the convolution

$$(\mathscr{G}^*_n \star \mathscr{G}_m)(k'_-) \equiv \int \frac{\mathrm{d}Q_-}{2\pi} \mathscr{G}^*_n(k'_- - Q_-)\mathscr{G}_m(Q_-). \tag{B5}$$

Comparing (B4) with (26) and (27) we find

$$\begin{aligned}\mathscr{A}^0_0 &= \mathscr{G}^*_0 \star \mathscr{G}_0, & \mathscr{A}^1_{\pm1} &= \mathscr{G}^*_0 \star \mathscr{G}_{\mp1} + \mathscr{G}^*_{\pm1} \star \mathscr{G}_0,\\ \mathscr{A}^2_0 &= \mathscr{G}^*_1 \star \mathscr{G}_1 + \mathscr{G}^*_{-1} \star \mathscr{G}_{-1}, & \mathscr{A}^2_{\pm2} &= \mathscr{G}^*_{\pm1} \star \mathscr{G}_{\mp1}.\end{aligned} \tag{B6}$$

The representation (B4) of the Compton amplitude together with (B5) furnishes another interpretation of the subpeaks in the Compton rate as the overlap of the momentum distributions of the incoming and outgoing Volkov states.

---

[1] A. Strickland and G. Mourou, Opt. Commun. **56**, 219 (1985).

[2] ELI project homepage: `http://www.extreme-light-infrastructure.eu`

[3] H. R. Reiss, J. Math. Phys. **3**, 59 (1962).

[4] A. I. Nikishov and V. I. Ritus, Zh. Eksp. Teor. Fiz. **46**, 776 (1963), [Sov. Phys. JETP **19**, 529 (1964)].

[5] A. I. Nikishov and V. I. Ritus, Zh. Eksp. Teor. Fiz. **46**, 1768 (1964), [Sov. Phys. JETP **19**, 1191 (1964)].

[6] A. I. Nikishov and V. I. Ritus, Zh. Eksp. Teor. Fiz. **47**, 1130 (1964), [Sov. Phys. JETP **20**, 757 (1965)].

[7] I. I. Goldman, Phys. Lett. **8**, 103 (1964).

[8] N. B. Narozhnyi, A. I. Nikishov and V. I. Ritus, Zh. Eksp. Teor. Fiz. **47**, 930 (1964), [Sov. Phys. JETP **20**, 622 (1965)].

[9] L. S. Brown and T. W. B. Kibble, Phys. Rev. **133**, A705 (1964).

[10] T. W. B. Kibble, Phys. Rev. **138**, B 740 (1965).

[11] K. T. McDonald (1986), preprint DOE/ER/3072-38; available as `www.hep.princeton.edu/~mcdonald/e144/prop.pdf`.

[12] R. C. Fernow et al. (October 27, 1989), DOE/ER/3072-55.

[13] Y. Y. Lau, F. He, D. Umstadter and R.Kowalczyk, Phys. Plasmas **10**, 2155 (2003).

[14] G. A. Mourou, T. Tajima and S. V. Bulanov, Rev. Mod. Phys. **78**, 309 (2006).

[15] Y. I. Salamin, S. X. Hu, K. Z. Hatsagortsyan and C. H. Keitel, Phys. Rept. **427**, 41 (2006).

[16] M. Marklund and P. K. Shukla, Rev. Mod. Phys. **78**, 591 (2006).

[17] V. I. Ritus, P. N. Lebedeva Akad. Nauk SSSR Vol. **111**, 5 (1979).

[18] T. Heinzl and A. Ilderton, Opt. Commun. **282**, 1879 (2009).

[19] T. J. Englert and E. A. Rinehart, Phys. Rev. A **28**, 1539 (1983).

[20] S.-y. Chen, A. Maksimchuk and D. Umstadter, Nature **396**, 653 (1998).

[21] M. Babzien et al., Phys. Rev. Lett. **96**, 054802 (2006).

[22] H. Schwoerer, B. Liesfeld, H.-P. Schlenvoigt, K.-U. Amthor and R. Sauerbrey, Phys. Rev. Lett. **96**, 014802 (2006).

[23] C. Bamber et al., Phys. Rev. D **60**, 092004 (1999).

[24] C. Bula et al. (E144 collaboration), Phys. Rev. Lett. **76**, 3116 (1996).

[25] D. L. Burke et al., Phys. Rev. Lett. **79**, 1626 (1997).

[26] E. S. Sarachik and G. T. Schappert, Phys. Rev. D **1**, 2738 (1970).

[27] E. Esarey, S. K. Ride and P. Sprangle, Phys. Rev. E **48**, 3003 (1993).

[28] R. L. Schoenlein et al., Science **274**, 236 (1996).

[29] K. Chouffani, D. Wells, F. Harmon and G. Lancaster, Nucl. Instr. and Meth. Phys. Research A **495**, 95 (2002).

[30] A. Debus et al., Proc. SPIE **7359**, 735908 (2009).

[31] W. P. Leemans et al., Phys. Rev. Lett. **77**, 4182 (1996).

[32] F. Sauter, Z. Phys. **69**, 742 (1931).

[33] FACET project home page: `http://facet.slac.stanford.edu/`

[34] G. A. Krafft, Phys. Rev. Lett. **92**, 204802 (2004).

[35] J. Gao, Phys. Rev. Lett. **93**, 243001 (2004).

[36] F. V. Hartemann, A. L. Troha, N. C. Luhmann Jr. and Z. Toffano, Phys. Rev. E **54**, 2956 (1996).

[37] T. Heinzl, D. Seipt and B. Kämpfer, Phys. Rev. A **81**, 022125 (2010).

[38] F. V. Hartemann and A. K. Kerman, Phys. Rev. Lett. **76**, 624 (1996).

[39] R. A. Neville and F. Rohrlich, Phys. Rev. D **3**, 1692 (1971).

[40] N. B. Narozhnyi and M. S. Fofanov, JETP **83**, 14 (1996).

[41] M. Boca and V. Florescu, Phys. Rev. A **80**, 053403 (2009).

[42] F. Mackenroth, A. Di Piazza and C. H. Keitel, Phys. Rev. Lett. **105**, 063903 (2010).

[43] J. Peatross, C. Müller, K. Z. Hatsagortsyan and C. H. Keitel, Phys. Rev. Lett. **100**, 153601 (2008).

[44] M. Ruf, G. R. Mocken, C. Müller, K. Z. Hatsagortsyan and C. H. Keitel, Phys. Rev. Lett. **102**, 080402 (2009).

[45] C. Harvey, T. Heinzl and A. Ilderton, Phys. Rev. A **79**, 063407 (2009).

[46] W. H. Furry, Phys. Rev. **81**, 115 (1951).

[47] P. Panek, J. Z. Kamiński and F. Ehlotzky, Opt. Commun. **213**, 121 (2002).

[48] V. B. Berestetsky, E. M. Lifshitz and L. P. Pitaevsky, *Relativistische Quantentheorie (Lehrbuch der Theoretischen Physik, Band 4),* Akademie Verlag Berlin, (1982).